Solar influences on Earth: past, present and future

(Fer Troulik/Unsplash/NASA/Goddard/SDO/J Hannah)

In his President's Address, given in May 2026, Mike Lockwood explores how our understanding of the Sun's influence on Earth has evolved, and how studies of exoplanets promise to place it in a wider astrophysical context

Understanding how the Sun influences Earth has been a central theme in space and climate science for over a century. In this article, I review how our understanding of Sun-Earth connections has developed, what current research reveals about these processes, and how studies of exoplanetary systems may help to place the Sun and Earth in a broader astrophysical context.

Past

Reconstructing past fluctuations in the Sun's influence on Earth is an area that I stumbled into, as member of a grant review panel. It is an example that I give to young researchers of the benefits to one's own science of contributing to peer review. On that panel, I was introduced to the *aa* geomagnetic index that was initially compiled for 1868–1968 by Jesuit priest Father Pierre-Noël Mayaud. It is now continued to the present day, covering over 157 years. My interest was sparked by the long-term variation revealed by *aa*. A literature search soon showed that Feynman & Crooker (1978) had made a serious attempt to exploit the longevity of the index.

They had used the correlation between *aa* and the product $B_S V_{SW}^2$, where B_S is the southward component of the interplanetary magnetic field, IMF $\underline{\boldsymbol{B}}$, in the geocentric solar magnetospheric frame, and V_{SW} is the solar wind speed. This correlation is understood because B_S facilitates power extraction from the solar wind through magnetic reconnection with the geomagnetic field, and the V_{SW}^2 term arises because the dominant energy in interplanetary space is the kinetic energy of the solar wind particles.

Feynman & Crooker examined how V_{SW} must have varied to explain the *aa* index variation if B_S was assumed constant. They were aware that this assumption was of limited validity. We devised a way to eliminate the assumption (Lockwood *et al.* 1999), using the fact that solar wind speed variations cause geomagnetic disturbances that recur every solar rotation (≈27 days), so the autocorrelation of *aa* at this period correlates very well with V_{SW}. In addition, we realised that although *aa* correlates strongly with B_S on short timescales, when averaged over a year, the IMF orientation factor B_S/B is essentially constant.

Through Parker spiral theory of the IMF, the ratio B_r/B could be computed, where B_r is the radial component of the IMF away from the Sun. Hence, we were able to compute the long-term variation in annual means of B_r from the *aa* data. However, B_r is a local parameter of the near-Earth heliosphere, and we were interested in a global solar parameter. The final piece of the jigsaw was the realisation that taking annual means averaged out the heliographic longitudinal structure in $|B_r|$, and that the Ulysses spacecraft had recently observed that $|B_r|$ was independent of heliographic latitude.

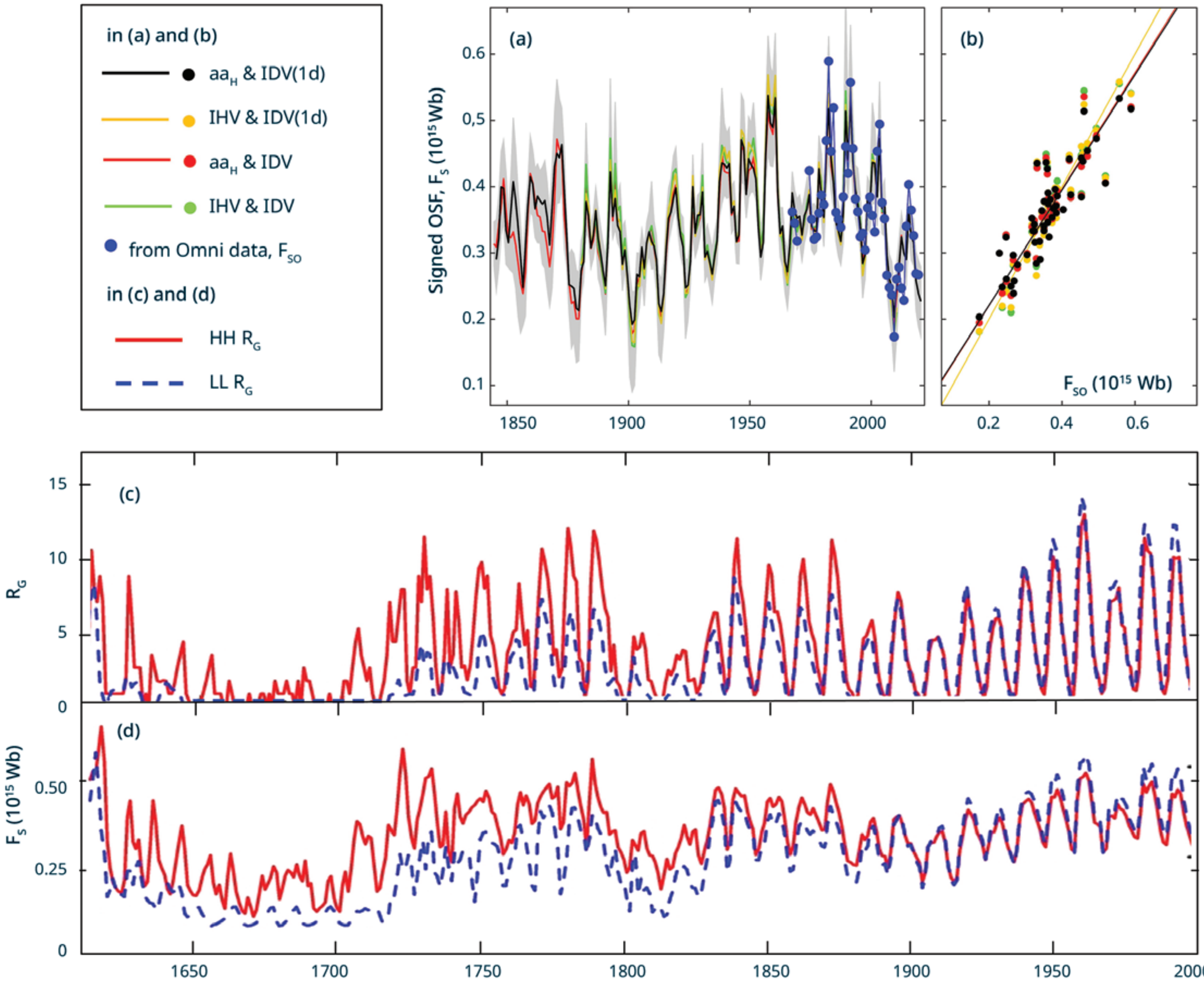

1 Reconstructions (Lockwood *et al.* 2022) of annual means of the signed OSF, F_S. (a) shows the reconstructions from four combinations of geomagnetic indices, using spacecraft observations F_{SO} from near-Earth interplanetary space, with correction for heliospheric 'switchbacks' (blue dots). (b) shows the relationships between the F_S and F_{SO} estimates. (d) shows these reconstructions extended back to 1600 using the cosmogenic isotope ^{44}Ti measured in meteorites (Asvestari *et al.* 2017). This reconstruction is made using the continuity equation for F_S, quantifying the source term using the HH and LL group sunspot number variations, R_G, shown in (c).

This empirical result is readily understood because close to the Sun the plasma β – the ratio of plasma to magnetic pressure – is small and magnetic pressure dominates. This means slightly non-radial flows equalise the tangential magnetic pressure, rendering the modulus of the radial field $|B_r|$ constant. Hence, our local B_r averages allowed us to compute the total signed solar magnetic flux threading a heliocentric sphere of radius $R_\oplus$ = 1 au, as $4\pi R_\oplus^2 <|B_r|>/2$. This was initially taken as an estimate of the signed open solar flux (OSF) leaving the top of the solar atmosphere and entering the heliosphere.

A lot of work was then undertaken to refine this result. There was considerable debate about the veracity of the drift in *aa*, largely due to misunderstandings of the method Mayaud (1972) had used in its compilation. This was definitively resolved by Lockwood *et al.* (2018), who used models of the intrinsic geomagnetic field to correct for the drift in magnetic latitude of each station before intercalibrating daily means as a function of time of year. This method resulted in aa_H, which unlike *aa*, has almost identical but independent variations from northern and southern hemisphere stations. Both *aa* and aa_H are 'range' indices, based on the range of variation in the horizontal field observed at a station over three-hour intervals. Other long-sequence geomagnetic activity indices, namely *IHV*, *IDV* and *IDV*(1d), have now been developed using hourly averages. They respond differently to solar wind and IMF conditions, a property that we can exploit.

Another complication is that, although $4\pi R_\oplus^2<|B_r|>/2$ is the signed flux threading a surface at the heliocentric distance r = $R_\oplus$, this exceeds the OSF, F_S, defined as the unsigned flux threading the 'coronal source surface' at the top of the solar corona. This is because field lines between the two can fold back on themselves – a phenomenon that has received much recent attention as 'switchbacks' in data from the Parker Solar Probe. After a variety of approximate corrections for the 'excess flux' this causes, a method was devised by Owens *et al.* (2017) and implemented by Frost *et al.* (2022). This method uses the fact that the hot corona generates a stream of 'strahl' electrons that always flow away from the Sun along magnetic field lines, so if the field lines are folded back on themselves, they are detected as strahl moving back towards the Sun. Thus, the amount of folded flux can be computed and the OSF accurately evaluated.

A further improvement was the realisation that, instead

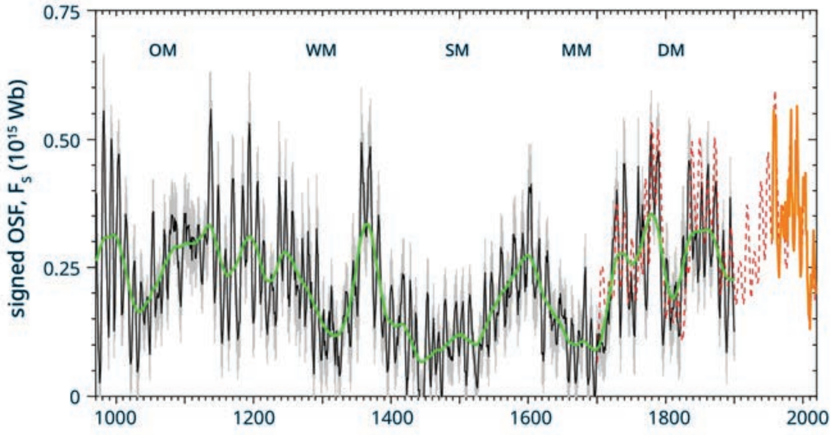

2 **The signed OSF, F_S, deduced from ^{14}C deposited in trees is shown (black), with the uncertainty band (grey) and smoothed running means (green). The reconstruction is calibrated from spacecraft data (orange, as shown in figure 1) and extended through modelled values from sunspot numbers fitted to geomagnetic data (dashed red line). From Usoskin (2023).**

of using the 27-day autocorrelation in *aa* to account for V_{sw}, a better method was to use different geomagnetic activity indices. In general, annual means of geomagnetic indices depend on BV_{sw}^n, where $n = 1.76$ for aa_H, slightly lower than the value of 2 initially found for *aa*, 1.68 for *IHV*, and –0.08 for *IDV*(1d) and –0.05 for *IDV*. Hence, by using combinations of indices for which *n* differs significantly, the variations in B, V_{sw} and F_S can all be computed. The result of these improvements can be seen in the review by Lockwood *et al.* (2022). The strong similarity of reconstructions from the four different combinations of geomagnetic indices with significantly different *n* is shown in figure 1(a), while figure 1(b) shows that they all agree well with the annual means of OSF derived from spacecraft data, F_{SO}, including the correction for folded field lines, as indicated by the blue dots in figure 1(a).

Hence, using historic geomagnetic data, together with understanding from space-age data extending back only to 1964, we have been able to reconstruct annual means of interplanetary parameters back to 1844. Recent work has increased the time resolution by over an order of magnitude by deriving means for each Carrington rotation of the Sun (Lockwood & Owens 2024).

“The ^{14}C record from trees can be used up until about 1950, when ^{14}C from atomic bomb tests swamped the record”

The more distant past

Using cosmogenic isotope abundances found in dateable terrestrial reservoirs, we can go back further in time. Beryllium-10 (^{10}Be), Carbon-14 (^{14}C) and Chlorine-36 (^{36}Cl) are generated as spallation or neutron-capture products of galactic cosmic rays (GCRs) striking atoms in our atmosphere. They inform us about OSF because the magnetic field in the heliosphere shields Earth from cosmic rays. Hence, the greater the OSF, the lower the abundances of cosmogenic isotopes. For long timescales, we must also account for changes in the geomagnetic field, as this also shields our atmosphere from GCRs (Usoskin 2023).

The ^{10}Be cosmogenic isotope is produced when GCRs with a broad range of energies impact atmospheric atoms. It is then attached to aerosols and precipitates into ice sheets, sediments and soils. It takes several weeks for ^{10}Be produced in the troposphere to be deposited, and about two years for ^{10}Be made in the stratosphere. Most ^{10}Be is deposited in polar ice sheets about a year after production. We cannot make reliable measurements of ^{10}Be abundances in ‘firn’, the intermediate state between fresh snow and compacted ice, but otherwise dateable ^{10}Be abundances can be determined from ice cores until relatively recent times.

^{14}C is different because carbon is exchanged between the atmosphere, the oceans and biomass in the carbon cycle. Trees incorporate atmospheric CO_2, including cosmogenic ^{14}C, during photosynthesis in the growing season; deposition in this reservoir then occurs 1–2 years after production and is smoothed over several years. Abundances can be determined from cores taken from ancient trees and from wood in historical buildings. The abundances must be analysed using a model that accounts for the carbon cycle if the production rate is to be determined (Zhang *et al.* 2022). The ^{14}C record from trees can be used up until about 1950, when ^{14}C from atomic bomb tests swamped the record.

Abundances of ^{36}Cl are lower, and there are competing production sources and chemical complications. It takes two years on average to be deposited because it is mostly formed in the stratosphere. These factors mean that ^{36}Cl data have lower time resolution than the annual resolution achievable with ^{14}C and ^{10}Be; however, it is most sensitive to lower-energy protons in the range 30–100 MeV, which helps to identify a solar, as opposed to galactic, origin of the causal particles. Like ^{14}C, ^{36}Cl is usable up to about 1950.

Figure 1(c) shows two reconstructions of the group sunspot number, R_G, labelled HH and LL and shown by red solid and blue dashed lines, respectively. These sequences differ before about 1820 because of uncertainties in intercalibrating observations from different observers. Using these R_G data, the highly successful continuity model of Solanki *et al.* (2000) is applied to compute the OSF. Figure 1(d) shows the resulting signed OSF computed from cosmogenic Titanium-44 (^{44}Ti) by Asvestari et al. (2017). Its ~60-yr half-life means that it formed on a meteorite during the final part of its journey to Earth, but the fall date must be known to allow for continuing decay on the ground. The Maunder Minimum (c1670–1710) can be seen in both OSF reconstructions, but it is deeper for the LL reconstruction. Reconstructions using ^{10}Be and/or ^{14}C can extend further back in time. Figure 2 shows a reconstruction extending back to 1000 CE, in which the Maunder Minimum is one of a sequence of grand minima, following the Oort (OM), Wolf (WM), and Spörer (SM) minima. The subsequent, shorter-lived Dalton Minimum (DM) is also labelled.

Reconstructions are possible back to about 7000 BCE, but these cosmogenic isotope data contain surprises. The biggest was discovered by Japanese PhD student Fusa Miyake, who found an event that occurred in 774 CE (Miyake 2012). Subsequently, similar confirmed spikes have been detected in dated records for 7176 BCE, 5259 BCE, 664–663 BCE and 993 CE. In addition, candidate events awaiting full confirmation have been identified for 12350 BCE, 5410 BCE, 1052 CE and 1279 CE.

What is astonishing about these events is the flux of energetic particles required to generate such large cosmogenic isotope abundances. The annual tree-ring record for the 774 CE event shows a ^{14}C increase of about 12 ppm, corresponding to a 1.2% increase in global atmospheric ^{14}C. This is roughly 20 times larger than the normal year-to-year variability, and the estimated global ^{14}C production during the event is approximately three to four times the normal annual production. Note that the carbon cycle reduces the ^{14}C signal and spreads it over subsequent years (Zhang *et al.* 2022).

Several non-solar mechanisms have been proposed, including supernovae, gamma-ray bursts, comet impacts, comet debris deposition, superflares from a nearby magnetar neutron star, and bursts of GCRs from nearby astrophysical accelerators. None of these provide satisfactory explanations. For example, comet theories are very unlikely because the ^{14}C spikes are very similar in ice cores from both poles, and gamma rays are also unlikely because isotope ratios – especially $^{36}Cl/^{10}Be$ – are better explained by proton-driven production than by gamma-ray cascades (Mekhaldi *et al.* 2015).

The one remaining explanation is extreme solar energetic particle (SEP) events, produced by very large solar flares and probably associated with extreme coronal mass ejections (CME). This scenario matches the observed production of different isotopes. Tree-ring records show a one-year jump, consistent with days of SEP bombardment. The difficulty for this proposed explanation is that the required particle fluence corresponds to an SEP event 30–100 times larger than the largest modern event.

The consensus is that Miyake events are indeed extreme SEP events, far larger than anything observed during the space age. Although very rare, the hazard inherent in these events is very large indeed. A Miyake event would cause widespread malfunctions and loss of spacecraft, degradation of solar panels, damage to electronics and navigation systems, and disruption or loss of weather and communication satellites. Radiation exposure for astronauts on the International Space Station would be severe, and exposure on lunar missions would likely be lethal. High-latitude aircraft would experience large radiation doses for passengers and crew, with polar flights diverted or grounded.

Such an event would not be extinction-level, as the atmosphere and geomagnetic field still provide strong shielding, so surface radiation flux increases would be small. An event of the size observed in 774 CE is estimated to occur roughly once every 1000 years on average.

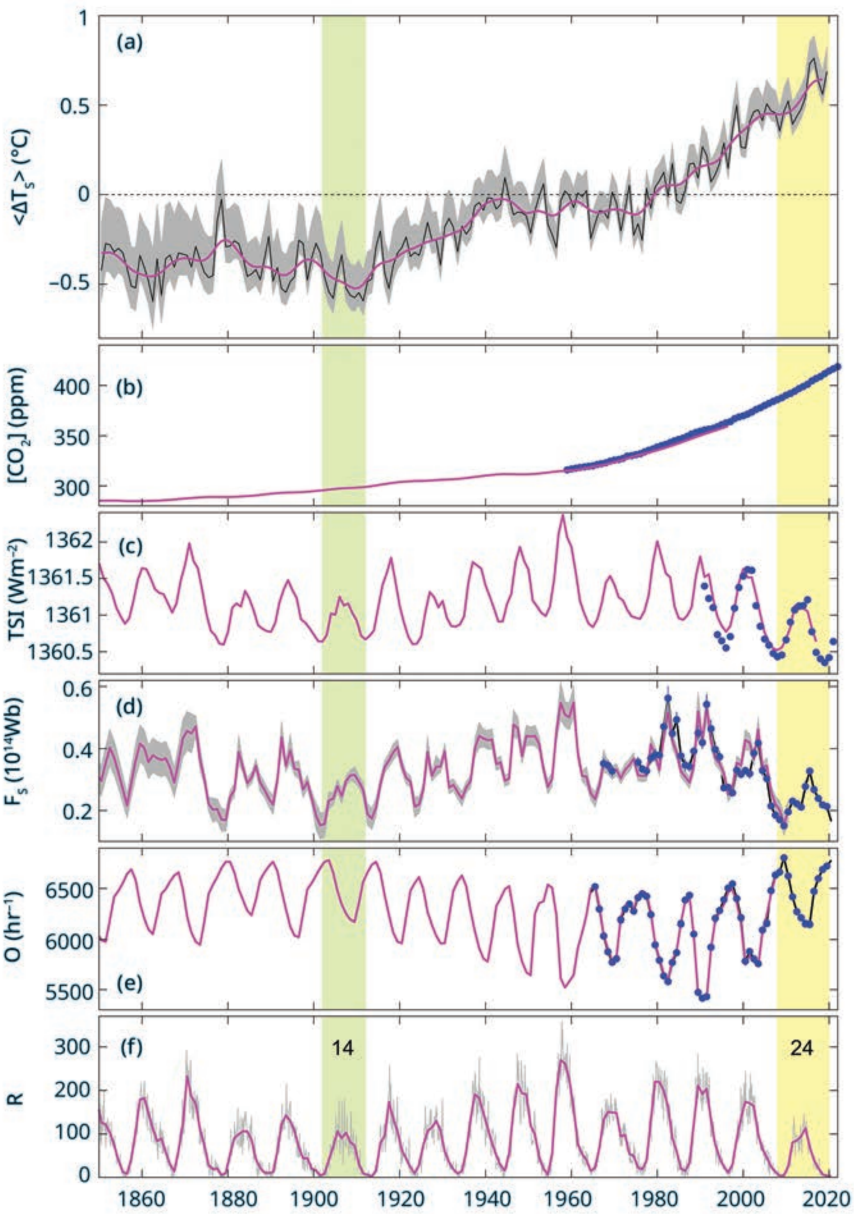

3 Variations in annual means of solar and heliospheric parameters compared with terrestrial climate change parameters. In each panel, the mauve line shows an historical reconstruction and the grey bands its 2-σ uncertainty; blue dots denote modern instrumental observations. Green and yellow vertical bands mark sunspot cycles 14 and 24, respectively. (a) The HadCRUT instrumental GMAST anomaly, relative to the 1980 value (Morice *et al.* 2012); the mauve line shows a 3-point running mean of the annual values (black); (b) Atmospheric carbon dioxide concentration, $[CO_2]$: the mauve line is from ice cores at Law Dome, Antarctica (Rubino *et al.* 2019) and observations from Mauna Loa, Hawaii (Keeling *et al.* 2009); (c) TSI reconstructed using the SATIRE-T model (Wu *et al.* 2018) and from the PMOD data composite; (d) Signed open solar flux, F_S, reconstructed by Owens & Lockwood (2012) and measured by Frost *et al.* (2022); (e) Cosmic ray flux, O, reconstructed by Usoskin *et al.* (2002) and measured at the Oulu cosmic ray station; (f) Monthly (grey) and annual (mauve) sunspot numbers, R, by Clette *et al.* (2023).

Present

There are a huge number of ongoing studies on the current state of solar influences on near-Earth space. These include understanding how large solar eruptions form and searching for precursors; probing the inner heliosphere and the origins of the solar wind; forecasting the structures and geoeffectiveness of CMEs; predicting the solar cycle and understanding the solar dynamo; investigating high-energy particle acceleration and their propagation to Earth; examining UT variations in the magnetosphere associated with the eccentric nature of the geomagnetic field; understanding preconditioning of geospace and compounding of events; analysing wave-particle interactions and loss processes in the radiation belts; quantifying the rapid acceleration of relativistic electrons; assessing solar forcing of the middle atmosphere; and determining what triggers magnetospheric substorms, including hemispheric differences. In all these areas, techniques such as ensemble modelling, skill scores, data assimilation, machine learning and AI are increasingly deployed. These are just a few examples of ongoing research that will continue and inform the studies discussed below in relation to exoplanets.

Instead of reviewing these many current activities, this section considers an application of the work described in the previous sections that helps confirm the drivers of the current state of Earth's climate. This debate dates to William Herschel, who identified an anticorrelation between sunspot number and the global market price of grain (Herschel 1801). His argument was that the sunspots decreased the Total Solar Irradiance (TSI) – the power per unit area at a distance 1 au from the Sun – thereby lowering global average temperatures, reducing grain yields and pushing up prices on global markets. There are many issues with this logic. For example, numerous factors influence market prices, and many others affect grain yields. However, the biggest problem with Herschel's idea is that we now understand that increased sunspot numbers cause a rise, and not a fall, in TSI.

Small changes in TSI arise from magnetic fields threading the solar photosphere. Sunspots are relatively large magnetic flux tubes, with typical diameters 2000–20000km, and the inhibition of upward heat transport by the magnetic field causes the temperature at the spot centre to be 3800–4200 K, compared with about 5770 K for the quiet Sun. As a result, they appear dark. On typical timescales of days to weeks, sunspot flux tubes disperse into smaller ones. Once their diameter falls below about 500 km, they appear as bright faculae, especially near the solar limb. This is because at these small diameters, the temperature in the flux tube is maintained by horizontal heat transport, but the density is lower because of magnetic pressure, allowing us to see deeper into the Sun. Near the solar limb, we observe the denser walls of these small flux tubes, which appear bright. This is often called the 'hot wall effect', although this is a misnomer, as it is the higher density of the flux tube walls that makes them brighter. The number of faculae is correlated with the number of sunspots, but their total area is an order of magnitude greater than that of sunspots. Hence, the brightening effect of faculae dominates over the darkening effect of spots (e.g. figure 1 of Lockwood & Ball 2020). Therefore, higher sunspot numbers cause slightly elevated TSI, rather than the decrease assumed by Herschel.

The claim that solar variability is the origin of climate change is a persistent one. Because the TSI determines the Global Mean Atmospheric Surface Temperature (GMAST) – a standard measure taken 2 m above the ground – people often assume that centennial variations in GMAST are caused by corresponding variations in TSI. However, TSI changes are too small for this to be the case. There is a simple reason for this: the solar convection zone (CZ) contains a mass of $\sim 3 \times 10^{28}$ kg, giving a thermal timescale of $\sim 10^5$ yr. Hence, over 100 yr, at most $\sim 10^{-3}$ of the CZ thermal energy could be released, giving a fractional solar luminosity change of the same order of magnitude. This yields a maximum climate radiative forcing of about 0.9 W m^{-2}, whereas the increase in greenhouse gas forcing over the same interval is about 2.3 W m^{-2}.

Climate scientists have long understood that solar variability is only a minor contributor to recent global warming compared to anthropogenic greenhouse gases (e.g. Jones *et al.* 2012). This is demonstrated by many detection-attribution studies using climate models, as well as by observational data sets that reveal a global downward trend in stratospheric temperatures while tropospheric temperatures have risen (e.g. Shangguan *et al.* 2019). This is a unique signature of greenhouse heat trapping between the stratosphere and troposphere, and inconsistent with a TSI increase that would have caused heating at all altitudes. Useful confirmation of this conclusion comes from comparing the time series of GMAST with various solar parameters, as shown in figure 3.

The OSF variations shown in figure 1 have been used to reconstruct TSI variations caused by magnetic field effects on the emissivity of the photosphere. The SATIRE suite of models is an evolution of the OSF model of Solanki *et al.* (2000) and integrates the emission from photospheric features at given locations on the solar disc. Figure 3 compares variations in key solar and climate parameters. Figure 3(c) shows TSI variations modelled using the SATIRE-T model by Wu *et al.* (2018), compared with values from spacecraft data. It should be noted that the reconstruction is calibrated using the PMOD TSI data composite, shown here by the blue dots only after the 'ACRIM gap' which makes the calibration of earlier data uncertain (see the review by Lockwood & Ball 2020).

"The biggest problem with Herschel's idea is that we now understand that increased sunspot numbers cause a rise, and not a fall, in TSI"

Figure 3 illustrates a point first highlighted by Lockwood & Frölich (2007): the period 1960–80 marked a turning point in solar activity, which had been rising since 1900, but subsequently declined such that by 2020 it had returned to the 1900 level. The grand maximum in long-term running means occurred in 1984 (Lockwood *et al.* 2022). Notably, GMAST rose both before and after the solar grand maximum. The rise in GMAST did pause between 1945–75, which is well understood as the cooling effect of sulphate aerosol pollution (Jones *et al.* 2012). The long-term variation in TSI, OSF and sunspot number are all consistent, and the variation in GCR flux, *O*, shows a strong anticorrelation with OSF.

The fact that the GMAST continued to rise after *O* reached its minimum during the grand solar maximum eliminates the much-discussed hypothesis that the temperature rise is due to GCRs seeding clouds. Clouds do have a major feedback effect on climate: they reflect incoming solar shortwave radiation, influencing Earth's albedo, but also contribute to the greenhouse effect by trapping outgoing longwave radiation and so can both cool and heat the planet. Their effect varies greatly with altitude, but the net effect of clouds is global cooling. Examining figures 2(d) and 2(e), we see that the rise in OSF between 1900 and 1960 reduced GCR fluxes. Hence, if clouds were seeded by GCRs, this would have decreased cloud cover and warmed the Earth. However, after 1990, GCR fluxes clearly rose again, which would be expected to have a cooling effect, yet GMAST values continued to rise.

It is instructive to compare solar cycles 14 and 24, highlighted in figure 3 by the green and yellow bands. In all the solar variations – sunspot number, OSF, TSI and GCR fluxes – these two cycles are very similar, yet figure 3(a) shows that GMAST was roughly one degree higher during cycle 24. The key difference between these cycles is the increase in greenhouse gas mixing ratios. For example, figure 2(b) shows that CO_2 concentrations rose from an average of 285 ppm during cycle 14 to 405 ppm during cycle 24, while analyses of air trapped in ice-sheet bubbles indicate pre-industrial levels were around 280 ppm.

Of course, global means do not reflect conditions at individual locations. Solar UV radiation variability influences the stratosphere, which is only a tiny perturbation to the global energy budget. However, some weather features, such as the jet stream, span the top of the troposphere and the bottom of the stratosphere and can be influenced by solar UV variability, producing regional variability (e.g. Woollings *et al.* 2010).

Like all scientific understanding, our knowledge of climate change can be described as a 'theory' and, as in all areas of science, acceptance of a theory is based on the consensus of scientists who specialise in that field, formed through peer review. Such a consensus is almost never completely universal. That climate change is currently being driven predominantly by anthropogenic activities is as near universal a scientific consensus as has ever been reached. Among those qualified to judge, the level of agreement

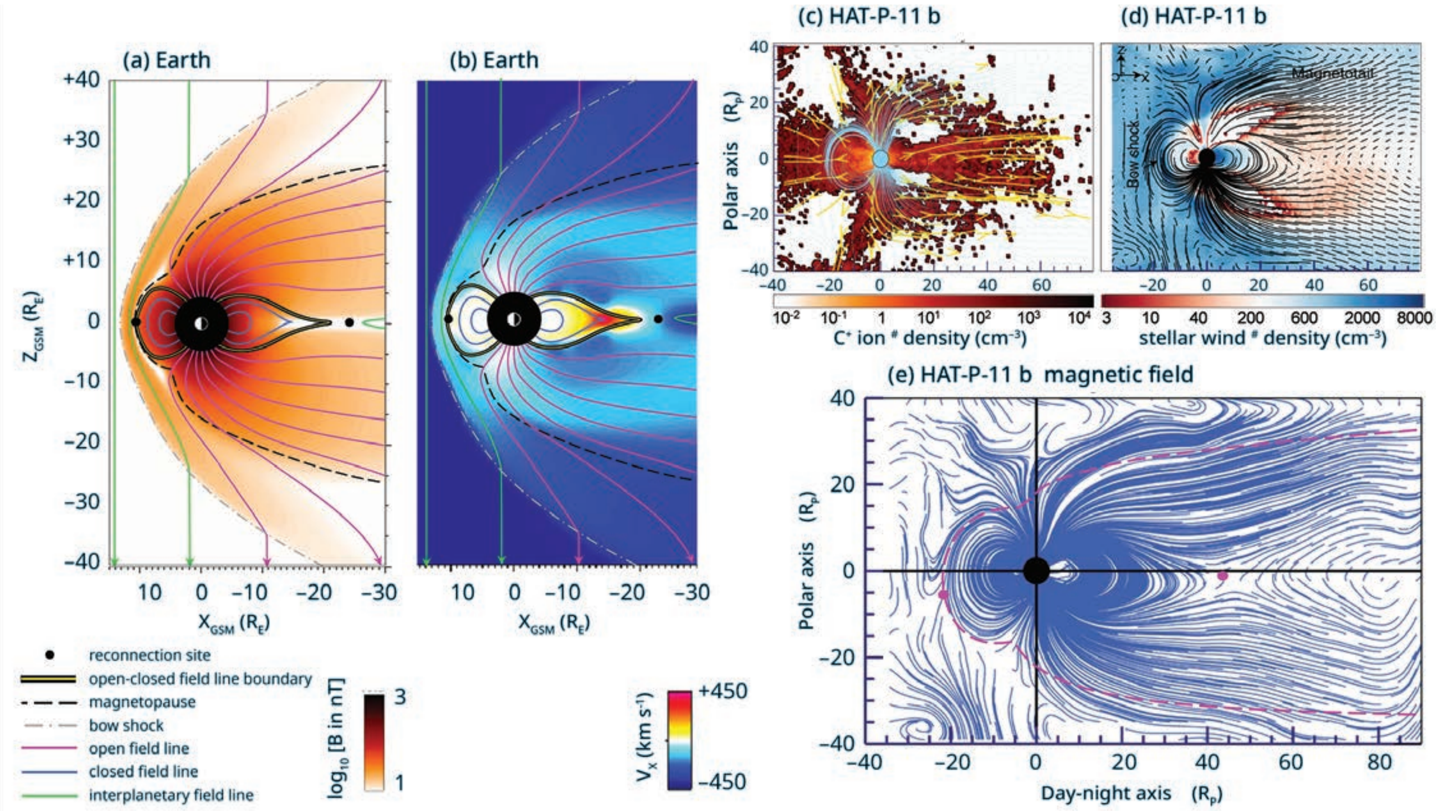

4 Application of Dungey's open magnetosphere model to exoplanets. (a) and (b) show global numerical model predictions of Earth's magnetosphere from simulations using the SWMF MHD model (Tóth *et al.* 2012) with a geocentric dipole model of Earth's intrinsic geomagnetic field and zero dipole tilt (from Lockwood 2023). (a) shows the magnetic field, *B*, on a logarithmic scale, and (b) shows the sunward plasma velocity, V_X. Mauve, blue and green lines indicate open, closed and interplanetary field lines, respectively. Mauve field lines that reach $X = -30R_E$ (where the mean Earth radius $1R_E = 6370$ km) are open because they thread the magnetopause at $X < -30R_E$. (c)–(e) are from analysis of the exoplanet HAT-P-11 b by Ben-Jaffel *et al.* (2022). (c) shows planetary C^+ (CII) ion abundances inferred from HST UV absorption spectra during transits; these ions are seen in the magnetosphere of the exoplanet, escaping from it along open field lines. (d) shows model-inferred magnetic field line segments superposed on a colour-coded plot of derived stellar wind proton number density. (e) shows the modelled magnetosphere of the exoplanet, which exhibits striking similarities to that modelled for the Earth.

is comparable to that for Einstein's theory of general relativity, which has passed every test that astronomers and cosmologists have applied to it. My personal, but firm, belief is that politicians who claim climate science is a 'scientific fraud' should never be granted stewardship of any part of the only habitable planet we know.

"My personal, but firm, belief is that politicians who claim climate science is a 'scientific fraud' should never be granted stewardship of any part of the only habitable planet we know"

Future

I will not attempt to predict the future of solar influences on near-Earth space or climate; however, I will discuss how we might learn more about them from exoplanets. Modelling work is already highlighting ways we could understand how orbit changes drive Milankovitch-cycle climate oscillations between ice ages and interglacials (e.g. Quarles *et al.* 2022).

On timescales of 10^8 years and greater, observations of many Sun-like stars provide insight into how the mass, rotation rate and magnetic field of our Sun will evolve. There have also been studies of how Earth's magnetosphere might respond to the resulting changes in the solar wind (e.g. Carolan *et al.* 2019). This work does not yet account for changes in Earth's magnetic field or for the fluctuations in the solar dynamo that produce grand minima in solar activity.

Looking ahead to millennia, centuries and even decades, we cannot yet predict the evolution of solar activity. At present, the rise and peak of a solar cycle can be predicted quite accurately from the open solar flux during the preceding sunspot minimum. However, in the declining phase of the cycle, unexpected events occur almost at random. During this time, the 'butterfly diagram' shows that sunspots start to appear near the solar equator, and this appears to introduce unpredictability into the second half of the solar cycle and subsequent cycles.

Small eddies and diffusion can move sunspots that emerged in one hemisphere into the other, causing them to evolve in an unexpected way. In addition, magnetic reconnection between emerged loops in opposite hemispheres can generate field-line 'bridges' between the two hemispheres. These seemingly small phenomena appear to have a disproportionate effect on the evolution of the solar magnetic field (Cameron *et al.* 2013; Lockwood *et al.* 2017).

A central limitation in understanding the long-term evolution of the Sun–Earth system is that we possess only a single example, and detailed observations of that example span only recent decades. Prior to this, we have only a few historic observation proxies, cosmogenic isotope records and remanent magnetisation in solidified lava flows. Exoplanets orbiting nearby Sun-like stars provide a natural time series for studying solar evolution (Gonzalez 2025), and magnetised rocky exoplanets offer the possibility of observing stellar wind-magnetosphere interactions across evolutionary sequences.

Figure 4 presents an exciting example: a 'hot-Neptune' exoplanet in close orbit around a K-type star, which is cooler and smaller than our Sun, a G-type star (Ben-Jaffel *et al.* 2022). The paper employs UV absorption spectra measured by the Hubble Space Telescope during planetary transits across the stellar disc, combined with understanding of Earth's magnetosphere, the Dungey cycle, and numerical modelling, to infer the structure of the planet's magnetosphere. It is quite astonishing to think that our model of Earth's magnetosphere has taken a century to develop, with its boundaries just

3 × 10^{-9} pc away, yet figure 4 provides a plausible depiction of a magnetosphere 38 pc away! Future studies of this type will be possible using the Plato mission, which will combine transit observations with stellar data from a ground-based array of asteroseismology detectors.

A key issue is how many candidate Earth-like exoplanet-stellar wind systems we will be able to observe. Occurrence rate estimates from the Kepler mission indicate that Earth-size planets (≈ 0.8–1.5 $R_{\oplus}$) at roughly Earth-like orbital distances (~ 0.8–1.5 au) around FGK stars occur at a rate $\eta_{(\oplus,1au)} \approx 14\% \pm 11\%$ (Petigura *et al.* 2013; Kunimoto & Matthews 2020). Note that in this section, uncertainty ranges span conservative to optimistic estimates.

The fraction of such planets capable of sustaining a magnetic dynamo is not yet known. Thermal evolution and dynamo-scaling models indicate that rocky planets with masses above about half an Earth mass can plausibly maintain core convection under Earth-like compositions (Driscoll & Olson 2011). This suggests that the dynamo-capable fraction may reduce the sample numbers by at most a factor of two. A reasonable working estimate is that 9% ± 8% of FGK stars host Earth-size planets at ~ 1 au capable of sustaining significant magnetic fields. Within 30 pc of Earth, there are approximately 2000 ± 200 FGK stars, based on modern nearby-star censuses derived from sources such as Gaia (Henry *et al.* 2018). This implies there could be 180 ± 160 nearby candidate Sun-Earth analogue systems for comparative studies of stellar wind-magnetosphere interactions. If we define a grand solar minimum as having an OSF level below 0.23 × 10^{15} Wb, figure 2 indicates that our Sun has been in such a state for about one-third of the last 950 years. This may be an usually high fraction, but some of these exoplanets are very likely orbiting stars currently in a grand minimum state.

Unlike transit spectroscopy studies, such as that shown in figure 4, which suffer from the low probability of geometric alignment (about $R_\star/a \approx 0.5\%$ for circular ~ 1 au orbits, where $R_\star$ is the stellar radius), radio diagnostics impose no alignment requirement; detectability is therefore limited by instrument sensitivity rather than geometry. Stellar wind mass-loss rates for solar analogues evolve in a known way (Johnstone *et al.* 2015), implying that young solar-type stars (0.5–1 Gyr) may drive winds up to about 30 times stronger than the present Sun. In the solar system, planetary auroral radio emission scales roughly with incident solar-wind power (the 'radiometric Bode's law', RBL; Zarka 2007), and Nichols & Milan (2016) have shown that RBL can be improved using the Dungey magnetospheric model. Enhanced winds should produce correspondingly stronger radio emission from planetary magnetospheres, meaning younger solar systems should be preferentially observable.

Facilities such as the Square Kilometre Array's Phase 1 low-frequency component (SKA1-Low) are designed to achieve microjansky sensitivities at 50–350 MHz (Braun *et al.* 2019). Model predictions suggest that present-day Earth analogues would be detectable only within a few parsecs, but stronger stellar winds or planetary magnetic fields could extend the detection horizon to roughly 8 ± 5 pc for Earth-mass planets and about 20 ± 10 pc for more strongly magnetised super-Earths (Grießmeier *et al.* 2007; Vidotto *et al.* 2015). Because the number of accessible systems increases with the volume of space surveyed, even modest increases in detection distance rapidly enlarge the observable sample.

By about 2030, early operations of SKA1-Low may enable the first direct detections – or strong constraints – on the magnetic fields of nearby giant exoplanets, primarily through direct planetary radio emission and potentially via initial Faraday-rotation experiments (Braun *et al.* 2019). After 2030, upgrades leading to SKA2 are expected to deliver roughly an order-of-magnitude improvement in radio sensitivity, along with much wider sky coverage and higher resolution, enabling far deeper studies of faint phenomena such as exoplanet magnetospheres.

The nearby (<30 pc) FGK stellar population spans ages from ≲ 0.1 Gyr to > 8 Gyr (Casagrande *et al.* 2011), providing a chronological sequence of solar-type wind evolution. As instrumental sensitivity improves and the detection horizon expands, the available stellar sample increases steeply. The number of local solar-type stars is already sufficient to support statistically meaningful studies once instrumental sensitivity reaches the required threshold. These studies open exciting possibilities, such as understanding solar wind-magnetosphere interactions during grand stellar activity minima and perhaps even during planetary main field reversals. ●

"As instrumental sensitivity improves and the detection horizon expands, the available stellar sample increases steeply"

AUTHOR

Mike Lockwood was President of the RAS between May 2024 and May 2026 and is a professor of space environment physics at the University of Reading.

REFERENCES

Asvestari E *et al.* 2017 *Mon. Not. R. Astron. Soc.* **467** 1608–1613
Ben-Jaffel L *et al.* 2022 *Nat. Astron.* **6** 141–153
Braun R *et al.* 2019 *Anticipated Performance of the Square Kilometre Array – Phase 1* (SKA1) arXiv:1912.12699
Cameron R H *et al.* 2013 *Astron. Astrophys.* **557** A141
Carolan S *et al.* 2019 *Mon. Not. R. Astron. Soc.* **489** 5784–5801
Casagrande L *et al.* 2011 *Astron. Astrophys.* **530** A138
Clette F *et al.* 2023 *Sol. Phys.* **298** 44
Driscoll P & Olson P 2011 *Icarus* **213** 12–23
Feynman J & Crooker N 1978 *Nature* **275** 626–627
Frost A M *et al.* 2022 *Sol. Phys.* **297** 82
Gonzalez G 2025 *Mon. Not. R. Astron. Soc.* **541** 3043–3072
Grießmeier J-M *et al.* 2007 *Astron. Astrophys.* **475** 359–368
Henry T J *et al.* 2018 *Astrophys. J.* **155** 265
Herschel W 1801 *Phil. Trans. R. Soc.* **91** 265–318
Johnstone C P *et al.* 2015 *Astron. Astrophys.* **577** A28
Jones G S *et al.* 2012 *J. Geophys. Res.* **117** D05103
Keeling R F *et al.* (2009) *Atmospheric Carbon Dioxide Record from Mauna Loa* data.ess-dive.lbl.gov/datasets/doi:10.3334/CDIAC/ATG.035
Kunimoto M & Matthews J M 2020 *Astrophys. J.* **159** 248
Lockwood M 2023 *J. Geophys. Res. Space Phys.* **128** e2023JA031671
Lockwood M & Ball W T 2020 *Proc. R. Soc. A* **476** 20200077
Lockwood M & Frölich C 2007 *Proc. R. Soc. A.* **463** 2447-2460
Lockwood M & Owens M J 2024 *Sol. Phys.* **299** 28
Lockwood M *et al.* 1999 *Nature* **399** 437-439
Lockwood M *et al.* 2017 *J. Geophys. Res. Space Physics* **122** 5870-5894
Lockwood M *et al.* 2018 *J. Space Weather Space Clim.* **8** A53
Lockwood M *et al.* 2022 *Front. Astron. Space Sci.* **9** 960775
Mayaud P-N 1972 *J. Geophys. Res.* **77** 6870–6874
Mekhaldi F *et al.* 2015 *Nat. Commun.* **6** 8611
Miyake F *et al.* 2012 *Nature* **486** 240–242
Morice C P *et al.* 2012 *J. Geophys. Res.* **117** D08101
Nichols J D & Milan S E 2016 *Mon. Not. R. Astron. Soc.* **461** 2353–2366
Owens M J & Lockwood M 2012 *J. Geophys. Res.* **117** A04102
Owens M J *et al.* 2017 *J. Geophys. Res. Space Phys.* **122** 980–10,989
Petigura E A *et al.* 2013 *Proc. Natl. Acad. Sci. USA* **110** 19273–19278
Quarles B *et al.* 2022 *Mon. Not. R. Astron. Soc.* **509** 2736–2757
Rubino M *et al.* 2019 *Earth Syst. Sci. Data* **11** 473–492
Shangguan M *et al.* 2019 *Atmos. Chem. Phys.* **19** 6659–6679
Solanki S K *et al.* 2000 *Nature* **408** 445–447
Tóth G *et al.* 2012 *J. Comput. Phys.* **231** 870–903
Usoskin I G 2023 *Living Rev. Sol. Phys.* **20** 2
Usoskin I G *et al.* 2002 *J. Geophys. Res. Space Phys.* **107(A11)** 1374
Vidotto A A *et al.* 2015 *Mon. Not. R. Astron. Soc.* **449** 4117–4130
Woollings T *et al.* 2010 *Geophys. Res. Lett.* **37** L20805
Wu C-J *et al.* 2018 *Astron. Astrophys.* **620** A120
Zarka P 2007 *Planet. Space Sci.* **55** 598–617
Zhang Q *et al.* 2022 *Proc. R. Soc. A.* **478** 20220497